Protection and Control of Modern Power Systems

ORIGINAL RESEARCH

Open Access

Designing of robust frequency stabilization using optimized MPC-(1+PIDN) controller for high order interconnected renewable energy based power systems

Muhammad Majid Gulzar*

Abstract

The challenge of controlling frequency becomes greater as the complexity of a power network increases. The stability of a power system is highly dependent upon the robustness of the controller. This paper presents automatic generation control (AGC) of a four-area interconnected power system along with integrated renewable energy sources of PV and wind energy. The designed model is a challenge given the increased penetration levels of PV and wind along with a thermal-hydropower system. The addition of a hydropower system as a fourth type results in the pole of the open loop system of the hydropower system being located at the right half side of the s-plan. This demands a robust control. A novel MPC-(1 + PIDN) is designed for high-order interconnected areas (HOIA) to stabilize the frequency in a robust way. The salp swarm algorithm is adopted to optimize the parameters of the PIDN controller. The performance of the proposed controller under HOIA is tested in a unbalanced load environment with uncertainty in the power system. The proposed controller can effectively handle the frequency disruption by stabilizing it in 0.86*s* for Area-1, 1.08*s* for Area-2, 0.81*s* for Area-3, and 0.84*s* for Area-4 with an average time of 0.89*s* for all the areas, whereas the average time for GWO: PI-PD, MPC/PI and GA-PI is 3.48*s*, 10.36*s* and 18.47*s*, respectively. The results demonstrate the effectiveness of the controller when compared to other controllers.

Keywords MPC-(1 + PID) controller, Salp swarm algorithm, High order interconnected area, Automatic generation control

1 Introduction

With soaring energy demand, renewable energy sources (RES) are becoming increasingly important. However, the integration of RES into the power system potentially increases frequency degradation. This needs to be countered by optimal controllers. Load frequency control (LFC) has been an important research area for stable operation of power systems [1]. The fluctuation in frequency is mainly due to imbalances in load and generation, and nonlinear factors like generation rate constraints (GRC) [2]. The foremost focus of the research is to ensure the stable operation of the generating power system by stabilizing the frequency. The role of LFC or automatic generation control (AGC) is to control the frequency and interchange of power over a tie-line among the interconnected areas to balance the load and generation [3, 4].

*Correspondence:
Muhammad Majid Gulzar
muhammad.gulzar@kfupm.edu.sa
Department of Control & Instrumentation Engineering, Interdisciplinary Research Center for Renewable Energy and Power Systems (IRC-REPS), King Fahd University of Petroleum and Minerals, Dhahran 31261, Saudi Arabia

1.1 Literature review

LFC has played an important role in confining the system frequency to a pre-specified limit, and has become a hot research topic because of the increasing challenges of the power system and the need for a robust controller. Studies examine the performance of the proposed controller in a highly complex network. There are many controllers for the LFC problem in the literature. PI/PID controllers are widely adopted for frequency stability. They are optimized by several algorithms, e.g., grey wolf optimization, but for complex power networks they exhibit sluggish response [5]. Different meta-heuristic techniques have been applied to different controllers to extract optimal tunable parameters for the controllers. The commonly applied algorithms in the field of AGC controller design are the bacterial foraging optimization algorithm (BFOA) [6], firefly (FA) [7], genetic (GA) [8], and others algorithms. In addition, other control formations have bee to improve effectiveness. In [9], an integral double derivative (IDD) controller is used for LFC with the help of a lighting searching algorithm (LSA). However, the addition of an extra derivative adds oscillations in the frequency response. The integral order (IO) [10], intelligent [11], and degree of freedom-based controllers which include 2DOF and the new 2DOF [12, 13], have been implemented in the field of LFC to enhance the performance of AGC.

For multi-area power systems, cascaded controllers are applied for LFC [14]. A GWO-based PI-PD controller is implemented, which has shown effective controllability [15], while the bat algorithm (BA)-tuned PD-PID is used for an electric vehicle to subdue frequency oscillations [16]. The Harris hawks optimization algorithm for PD-PID is applied in [17]. It shows promising results but the complexity of the algorithm is high. The hybrid stochastic fractal search and pattern search technique (hSFS-PS) for PI-PD controller is designed to enhance the controlling ability of the controller in [18]. The grasshopper algorithm (GOA) is used to optimize a PI-(1 + PD) controller for a multi-area power system in [19], while a multi-verse optimizing technique for PID + DD is implemented to monitor the usefulness of the controller in [20], but the complexity of the system is compromised. The aforementioned techniques have shown efficient results, but the testing system was fairly simplified and was mostly limited to a two-area system.

To overcome the limitations in the above controllers, several studies have proposed fuzzy/adaptive fuzzy-based PI/PID controller tuning but the attachment of a fuzzy controller makes it cumbersome [21, 22]. In [23], an internal model controller (IMC)-based PI controller is developed to cope with the LFC issue, while in [24], a dropout deep neural network with transfer learning technique is applied to ensure the optimal dispatch of AGC. Another dispatch technique, incorporating mileage, total generation and cost based on an MPC framework is proposed in [25], to maximize the Genco total profit by dynamic variation in the AGC. Likewise, a model predictive controller (MPC), which predicts the future behavior each time by minimizing the cost function, is the most extensively used controller in industry [26]. The importance of MPC is due to its fast response and robustness against the load disruption and uncertainty. The use of an MPC can be found in [27], where the MPC is deployed for a two-area thermal-thermal system and for PV-connected thermal systems. However, its performance is not analyzed in a complex network The MPC presents low overshoot with small steady-state error. The performance of MPC is tested for a plug-in hybrid electric vehicle along with a wind system in [28], while an adaptive MPC controller is also used for a PV-thermal two-area system to handle frequency fluctuations in a promising way [29]. In recent research, MPC-PI gain scheduling has been proposed for a renewable-based thermal interconnected two-area system for flexible operation of a power generating system [30]. Adaptive AGC mileage dispatch is proposed with renewable energy integration for better frequency regulation [31]. In [32], a four-area hydro-thermal design is proposed with the intelligent control design of PID, while a Fuzzy-PI controller with the integration of RES is proposed in [33] but the complexity of the studied network is not high. Active disturbance rejection control (LADRC) is designed for a four-area system to solve the problem of LFC, with a hydro-thermal area contained in the model [34].

1.2 Limitations of previous work and aims of the present study

The detailed literature review has indicated the following areas that need to be further investigated and thus has led to the proposed scheme in this paper:

(1) Conventional control techniques, e.g., PI/PID controllers, exhibit difficulties in reducing the uncertainty in the system. To improve the performance of the controller, a cascaded formation design has been introduced to overcome the challenge of system stability. However, the cascaded formations of the controller lack the ability to handle uncertainty robustly.
(2) Little attention has been devoted to analyzing the high complexity of the power system network, i.e., higher-order areas, and significant gaps exist in the analysis and performance of the controller designs for high-order areas.

(3) The newly formulated design MPC-(1 + PIDN) is devoted to enhancing the control ability of the previous (1 + PID) controller. The aim is to alleviate the frequency fluctuations robustly by applying the combination of prediction and conventional control techniques mainly for the higher-order area-based power system.

1.3 Innovation and contribution

The limitations in previous studies have paved the way for the following innovations in this paper:

(1) Formulation of high-order interconnected areas (HOIA), e.g., a combination of four areas, where the complexity of the area is enlarged by penetrating RES in the power system.
(2) For the HOIA system, the MPC-(1 + PIDN) controller is designed whereby the tunable parameters of the controller are obtained from SSA. The cascaded design applies the property of prediction based on the system constraints. These switch the operating state of the 1 + PIDN controller.
(3) The additional advantages of this type of controller as compared to PID are its robustness and ability to handle constraints while countering the noise.

This rest of the paper is organized as follows: Sect. 2 describes the system modeling, in which detailed modelling of wind, PV, thermal power system and hydropower system is established. Section 3 details the design of the proposed MPC-(1 + PIDN) controller, while in Sect. 4, the simulation results of the proposed technique under a complex system model are shown. Section 5 concludes the work.

2 System under investigation

Generally, frequency instability is due to the difference in demand and active power generation. The LFC mechanism is used to maintain the balance between load and generation, while the model of LFC is characterized by uncertainty and nonlinearity. The four-area power system model is depicted in Fig. 1, where the power-sharing among the areas takes place through tie-lines. The model contains three thermal areas along with PV and wind, while the fourth area contains a hydropower system and is also fed with PV and wind.

2.1 Thermal system modeling

The thermal generator consists of a governor, generator, steam turbine and re-heater. It also comprises of nonlinearity factors like generation rate constraint (GRC) and

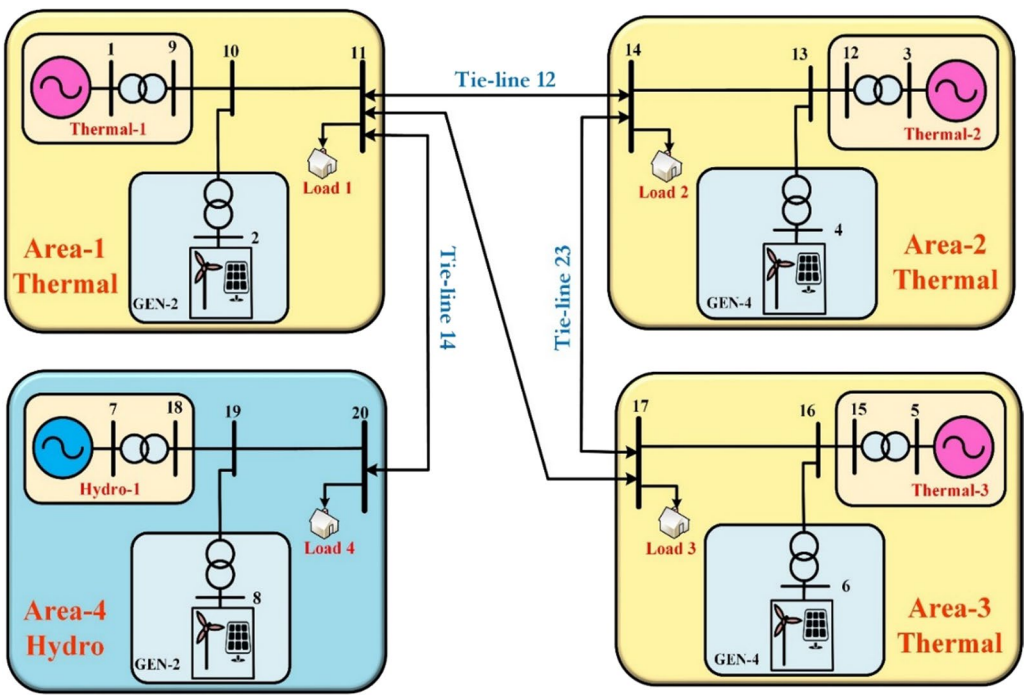

Fig. 1 Four-area power system model under investigation

droop [34]. The governor controls the mechanical motion of the turbine while maintaining valve operation and recovering the re-heater lost energy. Droop performs the function of controlling the speed of the prime-mover that is attached to the generator which converts mechanical energy into electrical energy [35]. The installed system is rated at 2000MW where the nominal operational load is 1000MW in each area. The assumed base power is 1000MVA.

The governor output $\Delta P_{gi}(s)$ is the difference of the reference power ΔP_{ref} and frequency change $\Delta f_i(s)$ passed through droop control $\frac{1}{R}$, as:

$$\Delta P_{gi}(s) = \Delta P_{ref}(s) - \frac{1}{R}\Delta f_i(s) \tag{1}$$

Power transfer between the areas (i and j) can be summarized as:

$$\Delta P_{tieij} = \sum_{j=1}^{n} \frac{T_{ij}}{S}\left(\Delta f_i - \Delta f_j\right) i \neq j \tag{2}$$

Area central error (ACE) is stated as:

$$ACE_i = B_i \Delta f_i + \Delta P_{tie,ij} i \neq j \tag{3}$$

where B_i is the frequency bias factor parameter in p.u. of MW/Hz, and $\Delta P_{tie,ij}$ is the change of tie-line power between the two areas.

Output Δf_i is expressed as:

$$\Delta f_i(s) = G_p(s)\left[\sum_{j=1}^{n} \Delta P_{Rij} - \Delta P_{d,i} - \Delta P_{tie,i}\right] \tag{4}$$

where $G_p(s) = \frac{1}{M_i s + D_i}$

2.2 Hydro generator modeling

The fourth area comprises of a hydropower plant along with PV and wind energy resources. The hydropower plant contributes to meeting the energy demand of the overall power generating system, while the PV and wind also contribute to meeting the energy demand. The nominal operation load on the hydro power plant is 1000MW, while the installed capacity of the hydro power plant is 2000MW. The hydropower plant exchanges power with Area-1 that is further connected with Area-2 and Area-3.

The hydro turbine transfer function is expressed as:

$$G_t(s) = \frac{K_r T_r s + 1}{T_r s + 1} \cdot \frac{-T_w s + 1}{0.5 T_w s + 1} \tag{5}$$

For Area-4, the open loop transfer function can be written as:

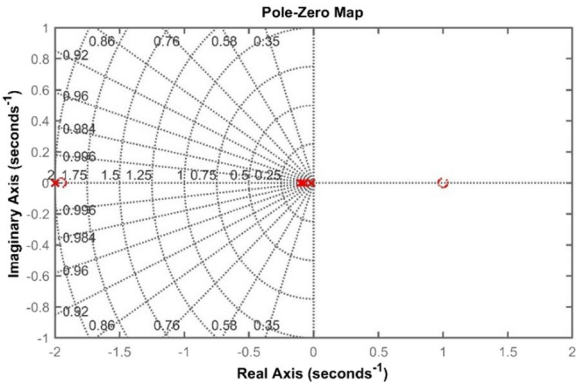

Fig. 2 Pole-zero mapping of the fourth area

Table 1 Model symbols

Terminology	Symbols	Values
Frequencybiasfactor	B_1, B_2, B_3, B_4	$0.425\frac{MW}{Hz}$
Speedregulationconstant	R_1, R_2, R_3, R_4	$2.4\frac{Hz}{MW}$
Generatorgain	$K_{p1}, K_{p2}, K_{p3} K_{p4}$	120 80
Generatortimeconstant	$T_{p1}, T_{p2}, T_{p3} T_{p4}$	20s 13s
Governortimeconstant	$T_{g1}, T_{g2}, T_{g3} T_1$	0.2s 48.7s
Hydroturbinetransmissioncoefficient	$T_2 T_3$	0.513s10s
Initialtimeconstantforwaterflow	T_w	1s
Reheattimeconstant	T_r	20s
Reheatgain	K_r	0.333

$$G(s) = \frac{K_{p4}(T_2 s + 1)(-T_w s + 1)}{(T_1 s + 1)(T_3 s + 1)(T_4 s + 1)(0.5 T_w s + 1)} \tag{6}$$

Figure 2 shows the pole-zero mapping of Area-4 as given in (6), with the zero on the right half plane making the system more difficult to control. The design of the robust controller is thus crucial for controlling the overall four-area system.

The model symbols along with their values are listed in Table 1

2.3 Photovoltaic system

The complexity of the power system in the four areas further increases because of PV penetration. PV is a DC nonlinear output source and is highly dependent on sun irradiation.

To connect PV generation to the power system, several conversions units are used. Figure 3 shows the designed PV model. These subsystems ensure that the PV runs at maximum power and transforms DC power into AC [36].

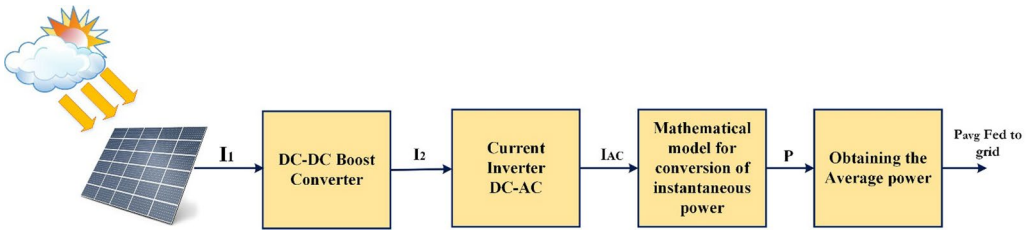

Fig. 3 PV system modeling

In the design, it is considered that PV is operating at its maximum power point [37]. The transfer function of the boost converter is given as:

$$g_1(s) = \frac{1}{m_1} \tag{7}$$

where m_1 is:

$$m_1 = \frac{v_2}{v_1} = \frac{i_1}{i_2} \tag{8}$$

Similarly, the inverter transfer function is denoted as:

$$g_2(s) = \frac{I_{ac}(s)}{I_2(s)} = \frac{s^2}{s^2 + \omega^2} \tag{9}$$

where $\omega = 2\pi f = 2\pi(50) = 314.12 rad/sec$.

The transfer function of the instantaneous power is given as:

$$P(s) = \frac{v_m i_m}{2s} + \frac{v_m i_m}{2} \frac{s}{s^2 + (2\omega)^2} \tag{10}$$

and the gain of the instantaneous power is provided as:

$$g_3(s) = \frac{p(s)}{I_{ac}(s)} = v_m \left(\frac{(s^2 + \omega^2)(s^2 + (2\omega)^2)}{s^2(s^2 + (4\omega)^2)} \right) \tag{11}$$

The average power is expressed as:

$$p_{avg}(s) = \frac{v_m i_m}{2s} \tag{12}$$

and the average power gain is described as:

$$g_4(s) = \frac{p_{avg}(s)}{p(s)} \tag{13}$$

2.4 Wind system

Wind energy meets the energy requirement via sharing the power through a tie line in an interconnected area. However, variation in the wind speed causes power imbalance and imposes disruption in frequency from the nominal value. In general, the interconnection or penetration of wind energy into the power system causes the LFC issue [38]. The modeling of the wind system is carried out and its schematic structure is depicted in Fig. 4. The mechanical output power of the wind turbine (WT) including the wake effect is expressed as [39]:

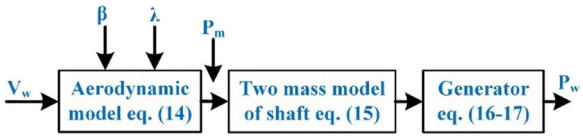

Fig. 4 Wind energy conversion model

$$P_w = \frac{1}{2} \rho A_T C_p(\lambda, \beta) V_{wake}^3 \tag{14}$$

where

$$\begin{cases} V_{wake} = V_m \left[1 - \sum_{i=1}^{n} \left(1 - \sqrt{\left(1 - \frac{F_T}{\rho \pi r^2 V_m^2} \right)} \right) \left(\frac{r}{r + k\Delta x} \right)^2 \right] \\ C_p(\lambda, \beta) = C_1 \left(\frac{C_2}{C_I} - C_3 \beta - C_4 \right) e^{\frac{-C_5}{\lambda_I}} + C_6 \lambda_T \\ \frac{1}{\lambda_I} = \frac{1}{\lambda + 0.08\beta} - \frac{0.035}{\beta^3 + 1}; \lambda_T = \frac{w_r r}{V_w}; A_T = \frac{\pi d^2}{4} \end{cases}$$

C_p is the power coefficient, β is the blade pitch angle, and ρ denotes the air density ($\frac{Kg}{m^3}$). The rotor diameter is represented by d (m), and the tip speed ratio (TSR) is denoted by λ_T, and λ_I is the intermittent TSR. F_T is the trust force, k denotes the decreasing coefficient (for onshore WT, k=0.075, and for offshore WT, k=0.05), Δx is the distance between two consecutive WTs, and V_w is the effective wind velocity.

The two-mass model of gear coupling is represented as [40]:

$$\begin{cases} \dot{\omega}_{WT} = -\left(\frac{D_{WT} + D_{shaft}}{J_{WT}} \right) \omega_{r,WT} + \left(\frac{D_{shaft}}{J_{WT}} \right) \omega_{gen} - \left(\frac{1}{J_{WT}} \right) T_{int} \\ \qquad + \left(\frac{1}{J_{WT}} \right) d(t) \\ \dot{\omega}_{gen} = \left(\frac{D_{shaft}}{2J_{WT}} \right) \omega_{r,WT} + \left(\frac{D_{gen} + D_{shaft}}{J_{gen}} \right) \omega_{gen} - \left(\frac{1}{n_{gear} J_{gen}} \right) T_{int} \\ \qquad + \left(\frac{1}{J_{gen}} \right) u(t) \\ \dot{T}_{int} = K_{shaft} \left(\omega_{WT} - \frac{\omega_{gen}}{n_{gear}} \right) \end{cases} \tag{15}$$

where J_{WT} and J_{gen} represent WT's moment of inertia of the rotor and generator, respectively. Shaft internal torque is represented by T_{int}, WT rotor and generator speed is denoted by $\omega_{r,WT}$, and gear turns ratio is represented by n_{gear}. D_{WT}, D_{shaft} and D_{gen} are the damping constant of the WT, coupling shaft and generator, respectively.

Assuming the output power P_w is ideal and the generator is lossless, thus there are [40]:

$$P_w = T_{gen}\omega_g \tag{16}$$

$$\frac{dT_{gen}}{dt} = \left(-\frac{1}{\tau_{gen}}\right)T_{gen} + \left(\frac{1}{\tau_{gen}}\right)T_{contol} \tag{17}$$

where τ_{gen} denotes the time constant of the generator, and T_{contol} represents the control torque that manipulates the output power of the WT against uncertain wind speed.

3 Proposed control strategy

The control operation of the four-area hybrid interconnected power system is designed. A robust control strategy is proposed where a cascaded design is formulated as MPC-(1 + PIDN) to deal with the LFC problem, originating from a mismatch in load and generation. The proposed controller contains the MPC that handles the constraints and minimizes the cost function robustly, while the (1 + PIDN) controller has the property of further expediting the controlling process by minimizing the settling time and handling disruption in frequency effectively. The MPC-(1 + PIDN) control structure is depicted in Fig. 5.

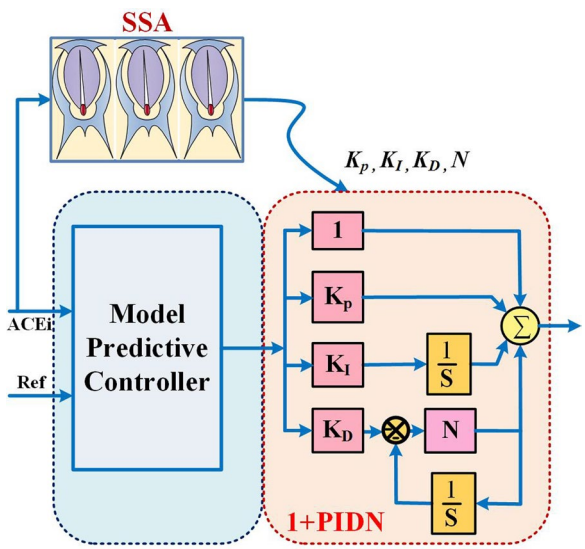

Fig. 5 MPC-(1 + PIDN) controller design

3.1 Design of MPC

The MPC controller is widely used in industry because of its robustness and was first introduced in 1978 [41]. In an MPC model, there are mainly three blocks, i.e.: predictive block, optimization solver, and cost function block. The function of these blocks is to shift the system response towards the reference trajectory based on the past and future predictions.

The output predictive vector is represented by $Y_p(k)$ as:

$$Y_p(k) = \phi Z(k) + \psi \Delta U(k) + \psi_I \Delta U_I(k) \tag{18}$$

The control law is obtained by the gradient descent method, i.e., $\frac{\partial J(k)}{\Delta U(k)} = 0$. To obtain the control law $u(k)$ the following equations are applied:

$$\Delta U(k) = \left(\psi^T Q \psi + R\right)^{-1} \psi^T Q\left(Y_r(k) - \phi Z(k) - \psi_I \Delta U_I(k)\right) \tag{19}$$

$$\Delta u(k) = \left(E_{N_u} O_{N_u(P-1)}\right)\Delta U(k) \tag{20}$$

$$u(k) = \Delta u(k) + u(k-1) \tag{21}$$

In the design of the cost function for the LFC problem, the constraint for the MPC is expressed as:

$$\begin{aligned} minJ(k) = min\Big\{ &\left(Y_p(k) - Y_r(k)\right)^T Q\left(Y_p(k) - Y_r(k)\right) \\ &+ (\Delta u(k))^T R(\Delta u(k)) \Big\} \end{aligned} \tag{22}$$

The parameters Q and R are the weighting vectors to balance the square future control and performance predictive error.

3.2 *Design of (1 + PIDN) and optimized by the Salp swarm algorithm*

The modified structure of the PID controller with a modified (1 + PIDN) is implemented. The gains of the (1 + PIDN) controller, i.e., K_P,K_I,K_D, are optimized by the salp swarm algorithm (SSA). The control signal $u(k)$ that is the output of the MPC is fed to (1 + PIDN), and the (1 + PIDN) controller processes the optimal signal of the MPC to further refine the signal to achieve the optimal control output for the LFC problem, as:

$$output = (1 + K_P + \frac{K_I}{s} + \frac{K_D N s}{N + s}) \times u(k) \tag{23}$$

where $u(k)$ is the output signal of the MPC.

3.2.1 *Salp swarm algorithm (SSA)*

The salp swarm optimization algorithm is designed from the transparent bodied slap which transforms itself into a chain-like structure during the search for food as proposed

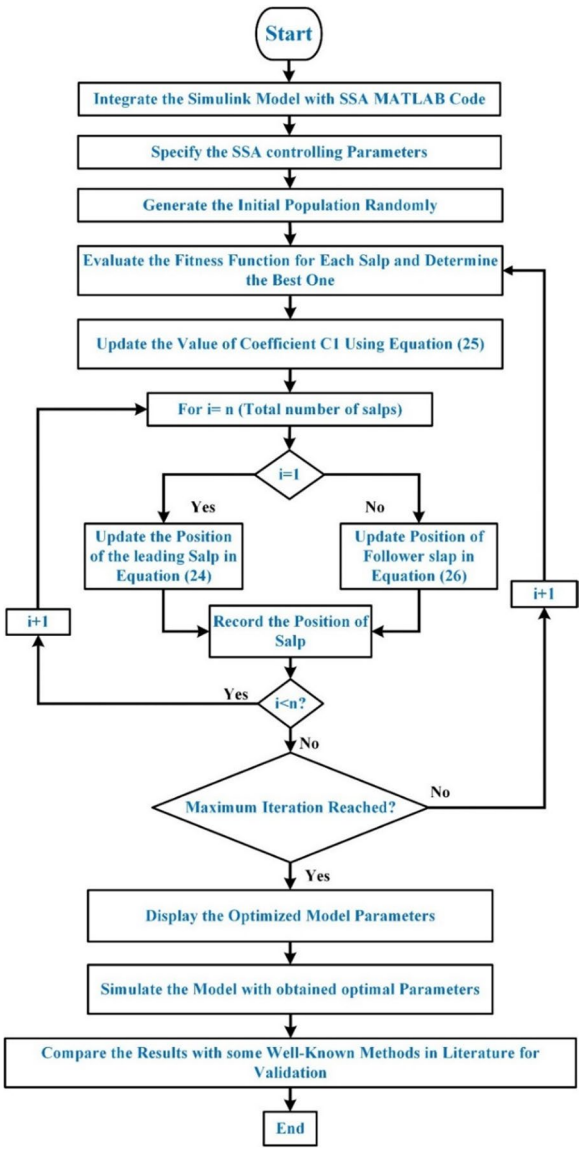

Fig. 6 Block diagram of SSA

Table 2 Algorithms parameters setting

Algorithm	Parameters
GA	Population size = 50, maximum generations = 100, crossover probability = 0.75, mutation probability = 0.1
GWO	Wolf number = 50, maximum iteration = 100, α = 0.7, ∀ = 0.9
SSA	Population size = 50, maximum iteration = 100, C2 = 0.5, C3 = 0.5
MPC	Prediction horizon P = 3, control horizon M = 2,

in [42]. SSA is mainly comprised of two sections: (i) leader and (ii) followers. The algorithm is translated in the form of a block diagram shown in Fig. 6.

The leader movement of the SSA is decided by:

$$K_j^i = \begin{cases} M_i + C_1\big((ub_j - lb_j)C_2 + lb_j\big), C_3 \geq 0 \\ M_i - C_1\big((ub_j - lb_j)C_2 + lb_j\big), C_3 < 0 \end{cases} \quad (24)$$

where M and K signify the target food and two-dimensional salp position, respectively. ub_j and lb_j denote the respective upper and lower bounds of the j^{th} dimension. Similarly, C_2 and C_3 are uniform coefficient numbers and C_1 is further expressed as:

$$C_1 = 2e^{-\left(\frac{4t}{t_{max}}\right)^2} \quad (25)$$

where t denotes the current iteration and t_{max} signifies the maximum number of iterations. The position is updated by:

$$K_j^i = \frac{1}{2}at^2 + v_0 t \quad (26)$$

Table 3 Optimized controller parameters

Controller parameters	GA-PI [8]	GWO:PI-PD [15]	MPC/PI [27]	MPC-(1 + PIDN)
Area-1	$K_P = -0.6130$ $K_I = -0.8010$	$K_P = -2.823$ $K_I = -2.789$ $K_P = -3.084$ $K_D = -1.997$	$K_P = 0.12$ $K_I = 0.81$	$K_P = 4.89$ $K_I = 7.710$ $K_D = 0.0148$ $N = 300$
Area-2	$K_P = -0.6911$ $K_I = -0.7665$	$K_P = -2.902$ $K_I = -3.627$ $K_P = -3.084$ $K_D = -0.982$	$K_P = 0.17$ $K_I = 0.92$	$K_P = 7.310$ $K_I = 12.927$ $K_D = 0.102$ $N = 300$
Area-3	$K_P = -0.6025$ $K_I = -0.7901$	$K_P = -3.1240$ $K_I = -3.1121$ $K_P = -3.0401$ $K_D = -0.8012$	$K_P = 0.20$ $K_I = 0.32$	$K_P = 2.267$ $K_I = 6.126$ $K_D = 0.0241$ $N = 300$
Area-4	$K_P = -0.6611$ $K_I = -0.8021$	$K_P = -2.8114$ $K_I = -3.6101$ $K_P = -2.1144$ $K_D = -1.1212$	$K_P = 0.11$ $K_I = 0.41$	$K_P = 6.589$ $K_I = 12.106$ $K_D = 0.0015$ $N = 300$

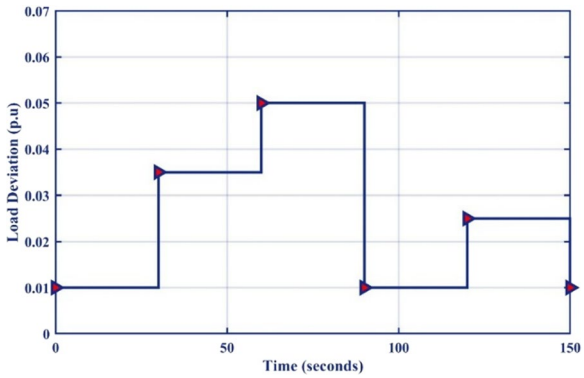

Fig. 7 Abrupt load deviation presentation

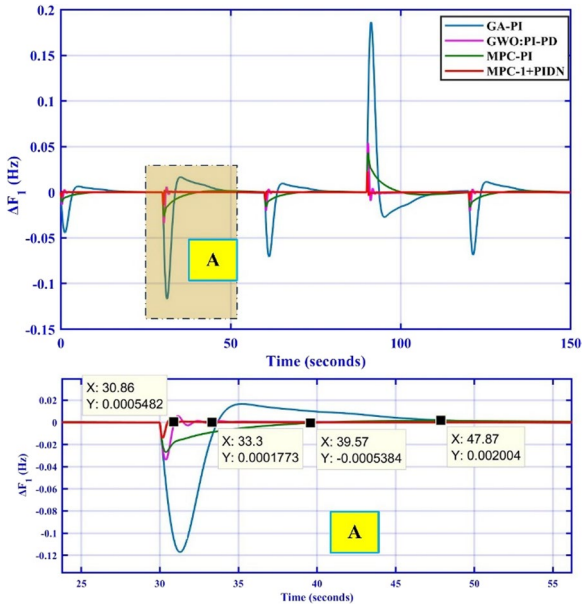

Fig. 8 Area-1 frequency response of the controller

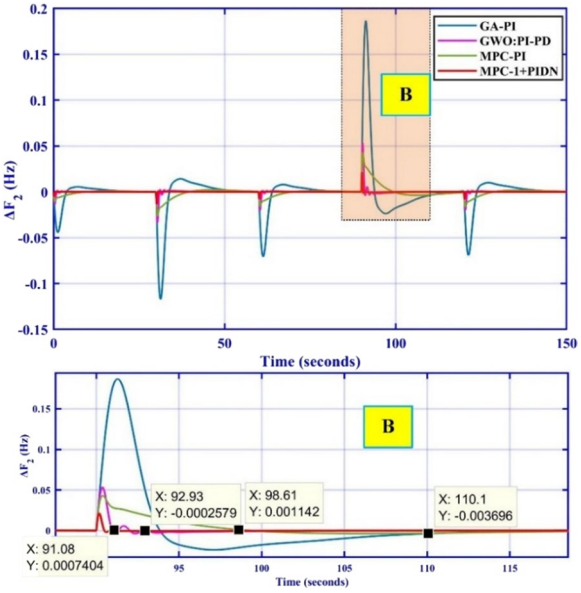

Fig. 9 Area-2 frequency response of the controller

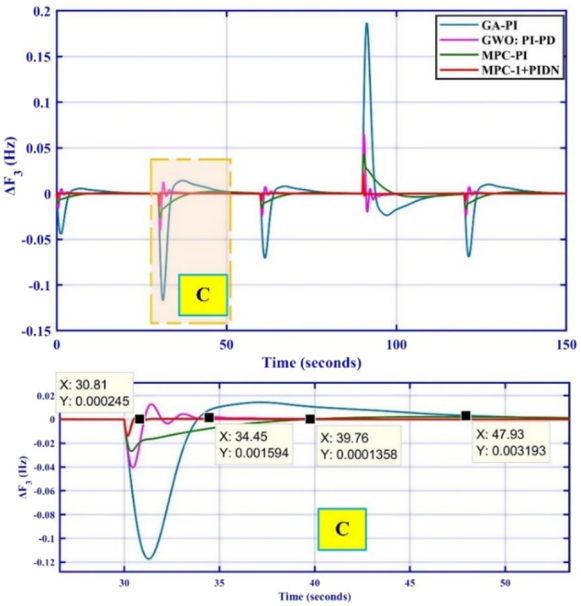

Fig. 10 Area-3 frequency response of the controller

4 Results and discussion

This section presents the effectiveness of the proposed control technique under HOA simulated in MATLAB 2017a, using a CoreTMi7 CPU at 2.2 GHz and 8 GB of RAM.

The initialization of the algorithms of GA, GWO, SSA, and MPC details are shown in Table 2. Moreover, the optimized controller parameters for the four-area based power system is formulated in Table 3.

After applying the setting in the simulation environment the performance of the proposed controller is simulated by applying the load perturbation as shown in Fig. 7. The load fluctuates between 1 and 5%, where 5% load is considered to be the worse load changing condition.

The frequency responses for Area-1, Area-2, Area-3 and Area-4 are depicted in Figs. 8, 9, 10 and 11, respectively. The proposed controller MPC-(1 + PIDN) shows robust results compared to other controllers, as it can effectively handle the frequency disruption by stabilizing under unbalanced loading. The highlighted parts of Figs. 8 and 9 are further explained to provide a better view of the responses obtained under the applied load condition. The effectiveness of the proposed controller on the fourth area which has a zero on the right half

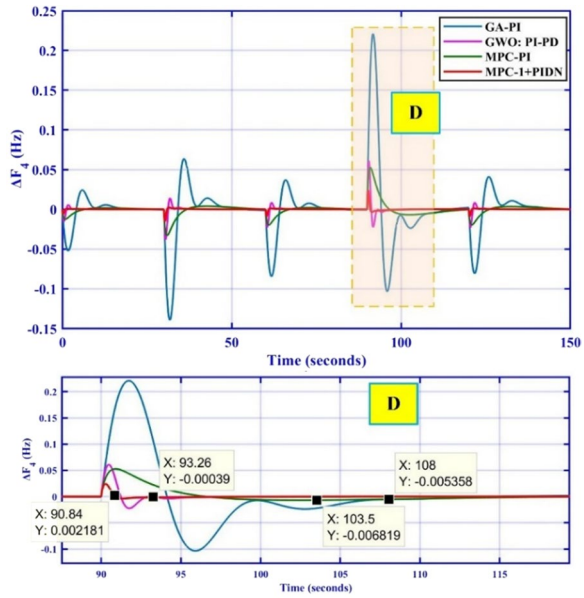

Fig. 11 Area-4 frequency response of the controller

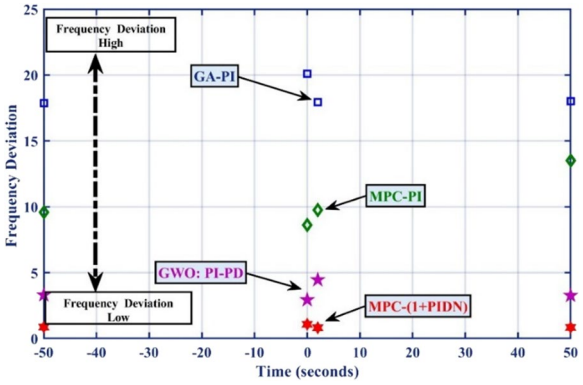

Fig. 12 Frequency deviation of the controllers

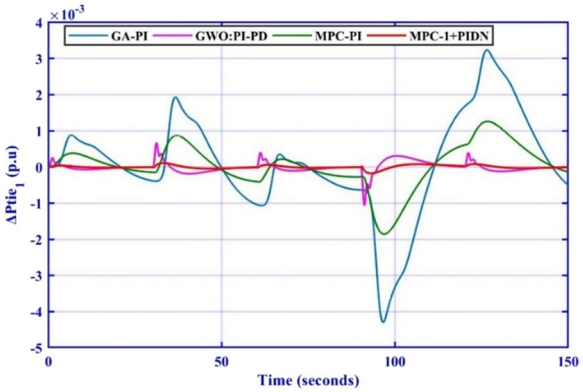

Fig. 13 Tie-line_12 response

plane requiring a robust controller for the handling of such issue, is also evident from Fig. 11. Overall, the proposed controller provides optimal results and handles the complexity of the four-area system effectively.

The results are compiled to analyze the effectiveness of the proposed controller and to compare with other state-of-the-art controllers as listed in Table 4. The deviations in frequency are plotted in Fig. 12. As seen, the proposed controller shows a minimum frequency deviation that is close to zero, while the other controllers have significant deviations. The tie-line power-sharing response of the controller is shown in Figs. 13, 14, 15, 16. The results indicate that the proposed controller shares the power effectively among the areas, while controllers such as FA-PI show an ineffective response.

The response time (ST) of the proposed MPC-(1 + PIDN) controller is 0.86s and has an undershoot response (US) of −0.001 for Area-1. In comparison, the response of GWO: PI-PD controller is 3.3s while also exhibiting US and an overshoot (OS) of− 0.03 and 0.01 respectively in Area-1. Similarly, the response of MPC/PI presents a settling time (ST) of 9.57s and a US response of− 0.03 with no OS. For Area-1, the response manifested by GA-PI is 17.87 *s* to settle the frequency fluctuation, while US and OS are− 0.18 and 0.01, respectively.

In the case of Area-2, the proposed controller shows an ST of 1.08*s* and OS of 0.01 with no US. In comparison, the ST, US and OS of GWO: PI-Pd are 2.93*s*, 0 and 0.05, respectively. In the case of the MPC/PI controller, the ST is 9.57*s*, US is− 0.03 with no OS. The GA-PI

Table 4 Performance analysis of the different controllers

Controllers	MPC-(1 + PIDN)			GWO:PI-PD [14]			MPC/PI [26]			GA-PI [8]		
	S.T	U.S	O.S	S.T	U.S	O.S	S.T	U.S	O.S	S.T	U.S	O.S
Area-1	0.86	− 0.001	0	3.3	− 0.03	0.01	9.57	− 0.03	0	17.87	− 0.18	0.01
Area-2	1.08	0	0.01	2.93	0	0.05	8.61	0	0.04	20.1	− 0.01	0.18
Area-3	0.81	− 0.01	0	4.45	− 0.04	0.01	9.76	− 0.02	0	17.93	− 0.18	0.01
Area-4	0.84	0	0.02	3.26	− 0.02	0.06	13.5	− 0.006	0.05	18	− 0.12	0.24

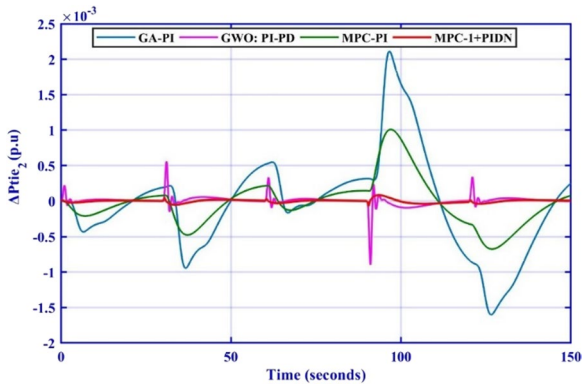

Fig. 14 Tie-line_23 response

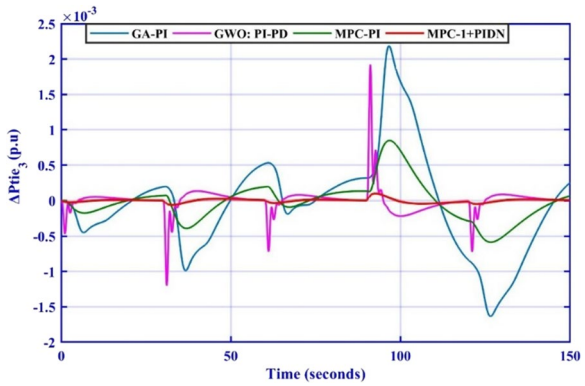

Fig. 15 Tie-line_13 response

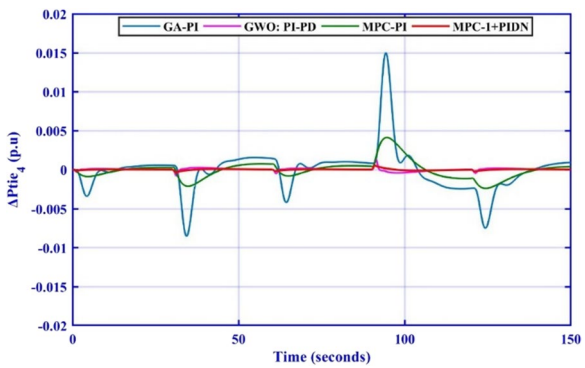

Fig. 16 Tie-line_14 response

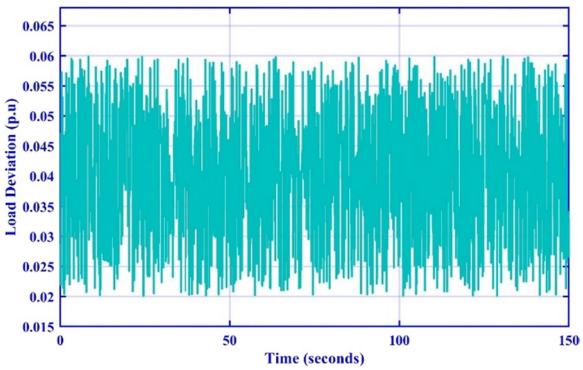

Fig. 17 Random load variation

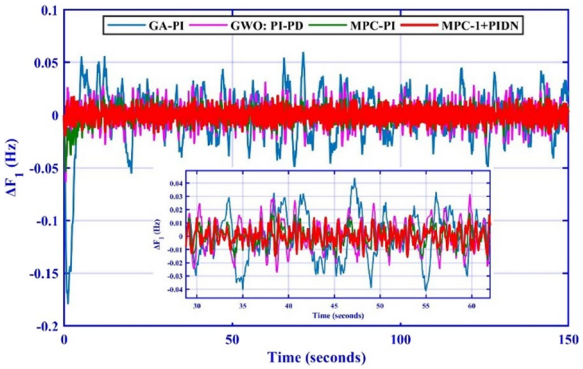

Fig. 18 Area-1 frequency response of the controller

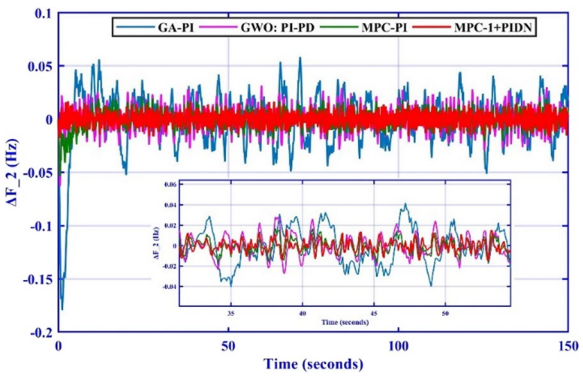

Fig. 19 Area-2 frequency response of the controller

controller shows ST of 20.1*s* and the responses of US and OS are − 0.01 and 0.18, respectively.

The simulated response of the MPC-(1 + PIDN) in Area-3 shows an ST of 0.81 s, US of − 0.01 with no OS. Similarly, in Area-3, the ST responses of GWO: PI-PD, MPC/PI and GA-PI are 4.45*s*, 9.76*s* and 17.93*s*, respectively. The US of the GWO: PI-PD, MPC/PI and GA-PI are − 0.04, − 0.02 and − 0.18, respectively. Further, the OS response of GWO: PI-PD is 0.01, while the MPC/PI presents no OS and GA-PI exhibits 0.01 OS response.

Finally, the responses of the MPC- (1 + PIDN), GWO: PI-PD, MPC/PI and GA-PI in Area-4 show STs of 0.84 *s*,3.26*s*, 13.5*s* and 18*s*, while the US are 0, − 0.02, − 0.006 and − 0.12, respectively. In case of the OS responses, the MPC- (1 + PIDN), GWO: PI-PD, MPC/PI and GA-PI depict 0.02, 0.06, 0.05, and 0.24, respectively.

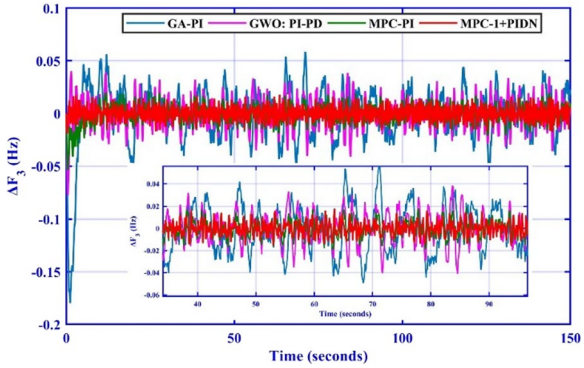

Fig. 20 Area-3 frequency response of the controller

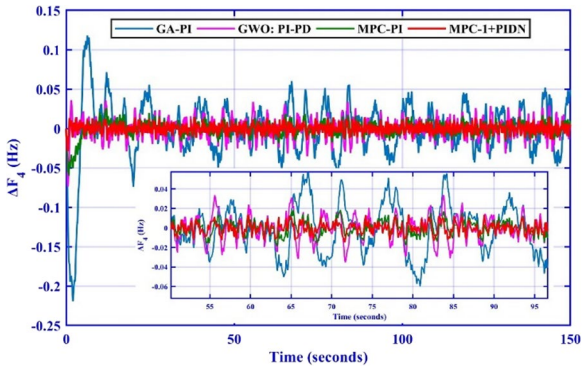

Fig. 21 Area-4 frequency response of the controller

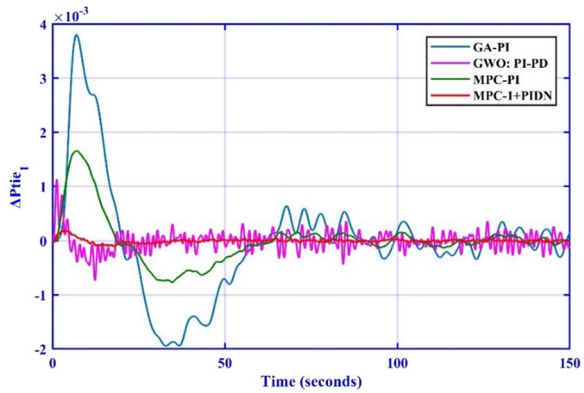

Fig. 22 Tie-line_12 response

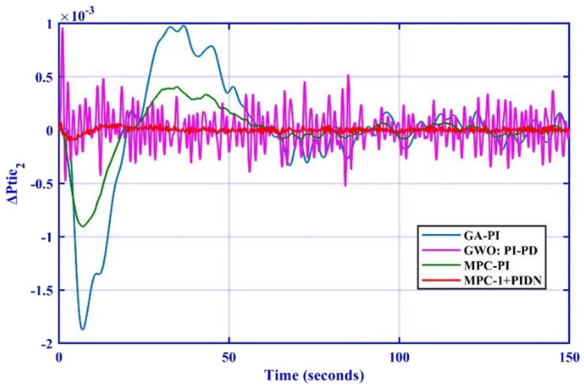

Fig. 23 Tie-line_23 response

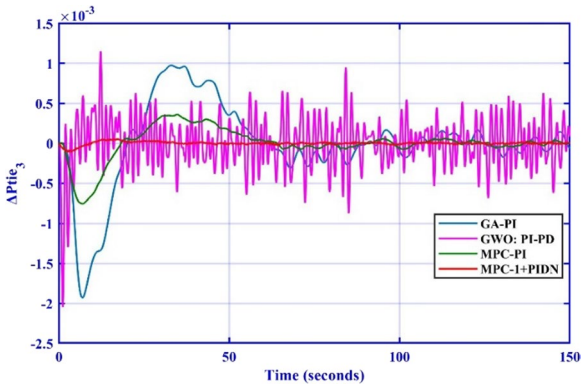

Fig. 24 Tie-line_13 response

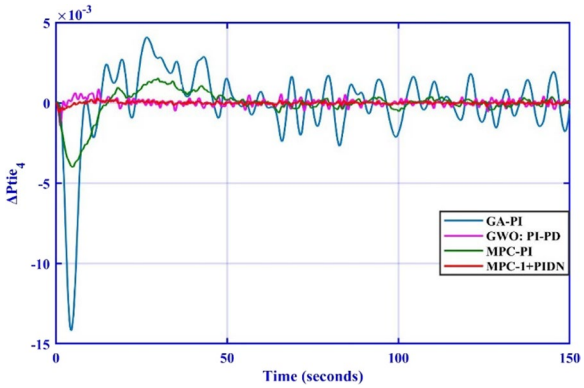

Fig. 25 Tie-line_14 response

The competence of the MPC–(1 + PIDN) controller is further tested by applying a random changing load between 1 and 6% variations as shown in Fig. 17. This load imbalance causes frequency distortion and leads to issues of system stability. As seen, the proposed controller demonstrates its robustness by suppressing the frequency fluctuation in minimum time compared to other controllers. The frequency responses in Areas1, 2, 3 and 4 are shown in Figs. 18, 19, 20, 21, respectively. The power between the adjoining areas is shared through a tie-line and the responses of the proposed controller show efficient sharing of power as sown in Figs. 22, 23, 24, 25.

The accumulations of the power from different sources such as PV and wind into the grid are shown in

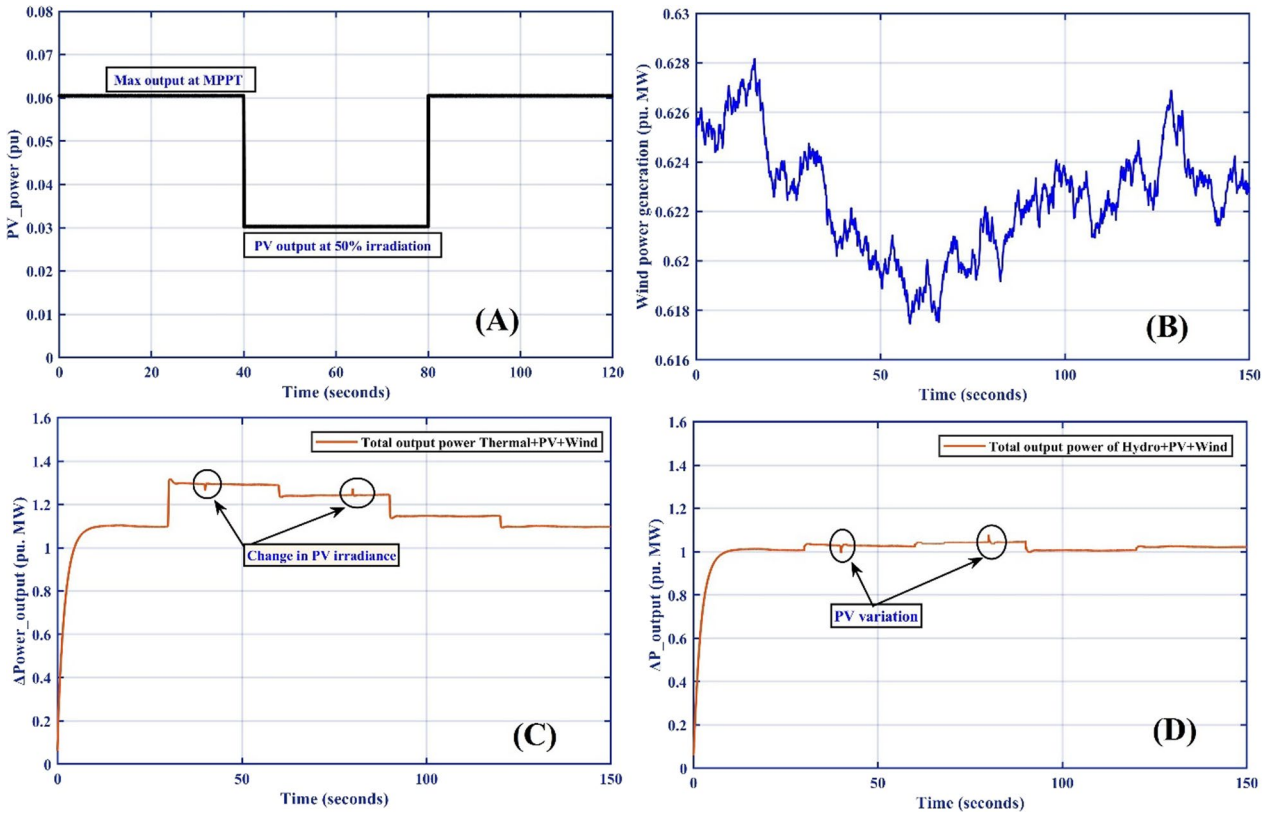

Fig. 26 Collective output power response **A** PV **B** wind **C** with thermal **D** with hydro

Fig. 26A and B, respectively, whereas the collective power responses of PV and wind into thermal and hydropower plants are shown in Fig. 26C and D, respectively.

5 Conclusion

The research aimed to design a control strategy for a high-order interconnected area (HOIA). The complexity of the HOIA is enhanced by penetrating the RES into the power system. The addition of the fourth area of a hydro-power plant causes a zero of the open loop system into the right half plane, and this makes control difficult. To handle such a complex network, a robust controller is required to suppress the frequency disruption due to load unbalance. A cascaded design with a combination of an MPC and 1 + PIDN is proposed. The designed controller MPC-(1 + PIDN) helps deal with the requirement of the HOIA system in a complex structure. It also mitigates the frequency fluctuation during load imbalance in less than 0.86*s* as compared to other controllers, e.g., 3.3*s* in case of GWO: PI-PD controller, 9.57*s* for MPC/PI controller and 17.87*s* for GA-PI controller, respectively. Finally, the effectiveness of the controller is investigated under different load-changing conditions and the proposed controller shows superiority over other state-of-the-art controllers.

In future studies, complex system designs will be considered, designs where the number of areas integrated may be enhanced to represent the increasing complexity of the power system network. Efficient and robust control designs will then be further discussed.

Acknowledgements
This publication is based upon work supported by the King Fahd University of Petroleum and Minerals. The author at KFUPM acknowledge the Interdisciplinary Research Center for Renewable Energy and Power Systems for the support received under grant no. EC221008.

Author contributions
All the work is done by the solo author. The author read and approved the final manuscript.

Funding
The author at KFUPM acknowledge the Interdisciplinary Research Center for renewable Energy and Power Systems for the support received under grant no. EC221008.

Availability of data and materials
Not applicable.

Declarations

Competing interests

The authors declare that they have no known competing financial interests or personal relationships that could have appeared to influence the work reported in this paper.

Received: 8 November 2022 Accepted: 14 March 2023
Published online: 25 March 2023

References

1. Dyak, A. A., Alsafasfeh, Q., & Harb, A. (2018). Stability analysis of connected large-scale renewable energy sources into Jordanian national power grid. *International Journal of Ambient Energy, 41*(9), 1016–1025. https://doi.org/10.1080/01430750.2018.1501742
2. Lu, K., Zhou, W., Zeng, G., & Zheng, Y. (2019). Constrained population extremal optimization-based robust load frequency control of multi-area interconnected power system. *International Journal of Electrical Power & Energy Systems, 105*, 249–271.
3. Gulzar, M. M., Iqbal, M., Shahzad, S., Muqeet, H. A., Shahzad, M., & Hussain, M. M. (2022). Load frequency control (LFC) strategies in renewable energy-based hybrid power systems: A review. *Energies, 15*(10), 3488. https://doi.org/10.3390/en15103488
4. Pathak, N., Ashu Verma, T. S., & Bhatti, I. N. (2019). Modeling of HVDC tie links and their utilization in AGC/LFC operations of multiarea power systems. *IEEE Transactions on Industrial Electronics, 66*(3), 2185–2197. https://doi.org/10.1109/TIE.2018.2835387
5. Guha, D., Roy, P. K., & Banerjee, S. (2016). Load frequency control of interconnected power system using grey wolf optimization. *Swarm and Evolutionary Computation, 27*, 97–115. https://doi.org/10.1016/j.swevo.2015.10.004
6. Panwar, A., Sharma, G., & Bansal, R. C. (2019). Optimal AGC design for a hybrid power system using hybrid bacteria foraging optimization algorithm. *Electric Power Components and Systems, 47*(11–12), 955–965.
7. Boddepalli, M. K., & Prema, K. N. (2018). Design and analysis of firefly algorithm based PID controller for automatic load frequency control problem. In *2018 Technologies for Smart-City Energy Security and Power (ICSESP)*, pp. 1–5. IEEE.
8. Hussein, T. (2012). A genetic algorithm for optimum design of pid controller in load frequency control. *World Academy of Science, Engineering and Technology, 70*, 956–960.
9. Rajbongshi, R., & Saikia, L. C. (2017). Combined control of voltage and frequency of multi-area multisource system incorporating solar thermal power plant using LSA optimised classical controllers. *IET Generation, Transmission and Distribution, 11*(10), 2489–2498.
10. Çelik, V., Özdemir, M. T., & Bayrak, G. (2017). The effects on stability region of the fractional-order PI controller for one-area time-delayed load–frequency control systems. *Transactions of the Institute of Measurement and Control, 39*(10), 1509–1521. https://doi.org/10.1177/0142331216642839
11. Golshannavaz, S., Khezri, R., Esmaeeli, M., & Siano, P. (2018). A two-stage robust-intelligent controller design for efficient LFC based on Kharitonov theorem and fuzzy logic. *Journal of Ambient Intelligence and Humanized Computing, 9*(5), 1445–1454.
12. Gupta, A., & Manocha, A. K. (2021). Designing of 2-degree of freedom load frequency controller for power system using novel improved pole clustering and genetic method of reduced-order modelling. *International Transactions on Electrical Energy Systems, 31*, e13063.
13. Karanam, A. N., & Shaw, B. (2022). A new two-degree of freedom combined PID controller for automatic generation control of a wind integrated interconnected power system. *Protection and Control of Modern Power Systems, 7*, 1–16.
14. El-Ela, A., Adel, A., El-Sehiemy, R. A., Shaheen, A. M., & Diab, A.E.-G. (2021). Enhanced coyote optimizer-based cascaded load frequency controllers in multi-area power systems with renewable. *Neural Computing and Applications, 33*, 8459–8477.
15. Padhy, S., Panda, S., & Mahapatra, S. (2017). A modified GWO technique based cascade PI-PD controller for AGC of power systems in presence of plug in electric vehicles. *Engineering Science and Technology, an International Journal, 20*(2), 427–442.
16. Dash, P., Saikia, L. C., & Sinha, N. (2015). Automatic generation control of multi area thermal system using Bat algorithm optimized PD–PID cascade controller. *International Journal of Electrical Power & Energy Systems, 68*, 364–372.
17. Barakat, M., Donkol, A., Hamed, H. F. A., & Salama, G. M. (2021). Harris hawks-based optimization algorithm for automatic LFC of the interconnected power system using PD-PI cascade control. *Journal of Electrical Engineering and Technology, 16*(4), 1845–1865.
18. Padhy, S., & Panda, S. (2017). A hybrid stochastic fractal search and pattern search technique based cascade PI-PD controller for automatic generation control of multi-source power systems in presence of plug in electric vehicles. *CAAI Transactions on Intelligence Technology, 2*(1), 12–25.
19. Latif, A., Suhail Hussain, S. M., Das, D. C., & Ustun, T. S. (2021). Double stage controller optimization for load frequency stabilization in hybrid wind-ocean wave energy based maritime microgrid system. *Applied Energy, 282*, 116171.
20. Guha, D., Roy, P. K., & Banerjee, S. (2017). Multi-verse optimisation: A novel method for solution of load frequency control problem in power system. *IET Generation, Transmission and Distribution, 11*(14), 3601–3611.
21. Cam, E., Gorel, G., & Mamur, H. (2017). Use of the genetic algorithm-based fuzzy logic controller for load-frequency control in a two area interconnected power system. *Applied Sciences, 7*(3), 308.
22. Gulzar, M. M., Sibtain, D., Murtaza, A. F., Murawwat, S., Saadi, M., & Jameel, A. (2021). Adaptive fuzzy based optimized proportional-integral controller to mitigate the frequency oscillation of multi-area photovoltaic thermal system. *International Transactions on Electrical Energy Systems, 31*(1), e12643.
23. Guha, D., Roy, P. K., Banerjee, S., & Purwar, S. (2022). Model order reduction of power systems and application of internal model control (IMC). In D. Guha, P. K. Roy, S. Banerjee, & S. Purwar (Eds.), *Application of intelligent control algorithms to study the dynamics of hybrid power system* (pp. 173–197). Springer Singapore. https://doi.org/10.1007/978-981-19-0444-8_7
24. Zhang, X., Li, C., Biao, X., Pan, Z., & Tao, Yu. (2023). Dropout deep neural network assisted transfer learning for bi-objective pareto AGC dispatch. *IEEE Transactions on Power Systems, 38*(2), 1432–1444. https://doi.org/10.1109/TPWRS.2022.3179372
25. Zhang, X., Zhao, Xu., Tao, Yu., Yang, Bo., & Wang, H. (2020). Optimal mileage based AGC dispatch of a GenCo. *IEEE Transactions on Power Systems, 35*(4), 2516–2526.
26. Rehiara, A. B., Yorino, N., Sasaki, Y., & Zoka, Y. (2019). A novel adaptive LFC based on MPC method. *IEEJ Transactions on Electrical and Electronic Engineering, 14*(8), 1145–1152. https://doi.org/10.1002/tee.22912
27. Gulzar, M., Rizvi, S., Javed, M., Sibtain, D., & Salah, R. (2019). Mitigating the load frequency fluctuations of interconnected power systems using model predictive controller. *Electronics, 8*(2), 156. https://doi.org/10.3390/electronics8020156
28. Jinquan, G., Hongwen, He., Jiankun, P., & Nana, Z. (2019). A novel MPC-based adaptive energy management strategy in plug-in hybrid electric vehicles. *Energy, 175*, 378–392.
29. Gulzar, M. M., Sibtain, D., Ahmad, A., Javed, I., Murawwat, S., Rasool, I., & Hayat, A. (2022). An efficient design of adaptive model predictive controller for load frequency control in hybrid power system. *International Transactions on Electrical Energy Systems, 2022*, 1–14. https://doi.org/10.1155/2022/7894264
30. Sibtain, D., Gulzar, M. M., Murtaza, A. F., Murawwat, S., Iqbal, M., Rasool, I., Hayat, A., & Arif, A. (2022). Variable structure model predictive controller based gain scheduling for frequency regulation in renewable based power system. *International Journal of Numerical Modelling: Electronic Networks, Devices and Fields*. https://doi.org/10.1002/jnm.2989
31. Zhang, X., Tan, T., Zhou, B., Tao, Yu., Yang, Bo., & Huang, X. (2021). Adaptive distributed auction-based algorithm for optimal mileage based AGC dispatch with high participation of renewable energy. *International Journal of Electrical Power & Energy Systems, 124*, 106371.
32. Prakash, S., & Sunil K. S. (2012). Four area load frequency control of interconnected hydro-thermal power system by intelligent PID control technique. In *2012 students conference on engineering and systems*, pp. 1–6. IEEE

33. Padhi, J. R., Debnath, M. K., & Kar, S. K. (2022). Self-tuning fuzzy-PI controller for load frequency control analysis with the integration of wind energy. *Energy Sources, Part A: Recovery, Utilization, and Environmental Effects, 44*(1), 613–631.
34. Zheng, Y., Sun, Q., Chen, Z., Sun, M., Tao, J., & Sun, H. (2021). Deep Q-network based real-time active disturbance rejection controller parameter tuning for multi-area interconnected power systems. *Neurocomputing, 460*, 360–373.
35. Parmar, K. P. S., Majhi, S., & Kothari, D. P. (2014). LFC of an interconnected power system with multi-source power generation in deregulated power environment. *International Journal of Electrical Power & Energy Systems, 57*, 277–286.
36. Podder, A. K., Roy, N. K., & Pota, H. R. (2019). MPPT methods for solar PV systems: a critical review based on tracking nature. *IET Renewable Power Generation, 13*(10), 1615–1632.
37. Bollipo, R. B., Mikkili, S., & Bonthagorla, P. K. (2020). Hybrid, optimal, intelligent and classical PV MPPT techniques: A review. *CSEE Journal of Power and Energy Systems, 7*(1), 9–33.
38. Iqbal, M., & Gulzar, M. M. (2022). Master-slave design for frequency regulation in hybrid power system under complex environment. *IET Renewable Power Generation, 16*(14), 3041–3057.
39. Guha, D., Roy, P. K., & Banerjee, S. (2021). Disturbance observer aided optimised fractional-order three-degree-of-freedom tilt-integral-derivative controller for load frequency control of power systems. *IET Gener Trans Distrib, 15*, 716–736.
40. Akhmatov ,V. (2003). Analysis of dynamic behavior of electric power systems with large amount of wind power (Ph.D. dissertation), Lyngby: Technical Univ Denmark; 2003.
41. Afram, A., & Janabi-Sharifi, F. (2014). Theory and applications of HVAC control systems–A review of model predictive control (MPC). *Building and Environment, 72*, 343–355.
42. Babaei, F., Lashkari, Z. B., Safari, A., Farrokhifar, M., & Salehi, J. (2020). Salp swarm algorithm-based fractional-order PID controller for LFC systems in the presence of delayed EV aggregators. *IET Electrical Systems in Transportation, 10*(3), 259–267. https://doi.org/10.1049/iet-est.2019.0076